ACS OMEGA

http://pubs.acs.org/journal/acsodf

Article

Molecular Insights into the Regulation of 3-Phosphoinositide-Dependent Protein Kinase 1: Modeling the Interaction between the Kinase and the Pleckstrin Homology Domains

Mireia Garcia-Viloca, Jose Ramón Bayascas,* José M. Lluch, and Àngels González-Lafont*

Cite This: *ACS Omega* 2022, 7, 25186−25199

Read Online

ACCESS | Metrics & More | Article Recommendations | Supporting Information

ABSTRACT: The 3-phosphoinositide-dependent protein kinase 1 (PDK1) K465E mutant kinase can still activate protein kinase B (PKB) at the membrane in a phosphatidylinositol-3,4,5-trisphosphate (PIP_3, PtdIns(3,4,5)P_3) independent manner. To understand this new PDK1 regulatory mechanism, docking and molecular dynamics calculations were performed for the first time to simulate the wild-type kinase domain−pleckstrin homology (PH) domain complex with PH-in and PH-out conformations. These simulations were then compared to the PH-in model of the KD−PH(mutant K465E) PDK1 complex. Additionally, three KD−PH complexes were simulated, including a substrate analogue bound to a hydrophobic pocket (denominated the PIF-pocket) substrate-docking site. We find that only the PH-out conformation, with the PH domain well-oriented to interact with the cellular membrane, is active for wild-type PDK1. In contrast, the active conformation of the PDK1 K465E mutant is PH-in, being ATP-stable at the active site while the PIF-pocket is more accessible to the peptide substrate. We corroborate that both the docking-site binding and the catalytic activity are in fact enhanced in knock-in mouse samples expressing the PDK1 K465E protein, enabling the phosphorylation of PKB in the absence of PIP_3 binding.

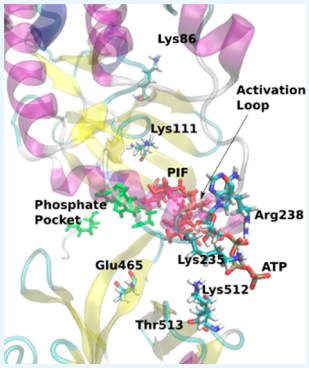

1. INTRODUCTION

3-Phosphoinositide-dependent protein kinase 1 (PDK1) is a key protein kinase that activates at least 23 members of the AGC (cyclic AMP-dependent kinases, cyclic GMP-dependent kinases, and protein kinase C) kinase family by phosphorylation. These include isoforms of protein kinase B (PKB, also known as Akt), p70 ribosomal S6 kinase (S6K), serum and glucocorticoid-induced protein kinase (SGK), p90 ribosomal S6 kinase (RSK), and isoforms of protein kinase C (PKC).[1] These proteins are phosphorylated by PDK1 at highly conserved Ser and Thr residues located at the T-loop (also known as activation loop) of the kinase domain (KD). The mammalian target of rapamycin (mTOR) complexes phosphorylate a critical Ser or Thr residue within the hydrophobic motif site, a highly conserved domain that represents a molecular signature for the AGC family members. Phosphorylation of both the T-loop and the hydrophobic motif residues is required for the maximal activation of those enzymes. The cascade of kinases initiated by PDK1 serves to propagate the phosphatidylinositol-3,4,5-trisphosphate (PIP_3, PtdIns(3,4,5)P_3) second messenger signal produced by the phosphoinositide 3 kinase (PI3-kinase) in response to insulin and growth factors.[2] Signaling pathways regulated by the phosphorylation of protein kinases are essential for many biological processes.[3] Uncontrolled PDK1 downstream signaling has been related with many different diseases.[4] Hence, PDK1 is overexpressed in a variety of human cancers, contributing to the proliferation, migration, and dissemination of tumor cells.[5] For this reason, PDK1 has become a target for cancer therapy.[6−9]

The modular architecture of PDK1 consists of a N-terminal Ser or Thr kinase domain (KD) and a C-terminal pleckstrin homology (PH) domain that binds to PIP3, phosphatidylinositol-3,4-bisphosphate (PtdIns(3,4)P_2, PIP2), and with lower affinity to phosphatidylinositol-4,5-bisphosphate (PtdIns(4,5)-P_2) at the plasma membrane. PDK1 possesses the intrinsic ability to autophosphorylate both its own T-loop at residue Ser241 within the KD and the Thr513 residue at the PH, which has been shown to be critical for PDK1 activation.[10] For this reason, PDK1 is considered a constitutively active kinase in mammalian cells.[11] Consequently, it was proposed first that 3-phosphoinositide lipids were only necessary to activate substrates for phosphorylation by PDK1.[12,13] However, there is now evidence for the acute activation of PDK1 itself, and many efforts have been dedicated to understanding the mechanisms of PDK1 regulation as well as those of the kinases that constitute its substrate-signaling network.[14]

Among the AGC family, PDK1 and PKB are the only members that possess PtdIns(3,4,5)P_3-binding PH domains.

Received: April 1, 2022
Accepted: June 23, 2022
Published: July 15, 2022

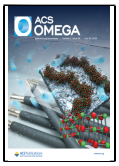

Numerous experiments in vitro and in cells suggested that the activation of PKB by PDK1 was precisely meant to rely on the mutual binding of the PDK1 and PKB PH domains to PtdIns(3,4,5)P_3; this interaction would mediate the translocation and colocalization of these two kinases at the plasma membrane, allowing a tight interaction and the phosphorylation of PKB by PDK1 at the Thr308 activating residue.[15,16] PKB binding to PIP3 does not really activate the PKB kinase but rather triggers a conformational change that facilitates the phosphorylation by PDK1. In live cells, this induced conformational change alters the interaction between the PH and KD domains, thus changing from an inactive PKB-in conformer in which the PH and KD domains establish close interactions that hide the activation sites to a PKB-out structure suitable for phosphorylation and activation.[17]

Interestingly, several studies have suggested a direct role for the binding of the PH domain of PDK1 to 3-phosphoinositides in activating the protein, possibly by inducing a conformational change like that of PKB.[10] In particular, the autophosphorylation of Thr513 in combination with the binding of the PH to PIP3 could trigger the structural modification that leads to the PDK1 active form. However, the regulation of PDK1 activity in live cells seems to depend on a homodimerization process rather than an intramolecular conformational change.[14,18] A computational model of the PDK1 full-length homodimer with an autoinhibitory PH−PH configuration was built using a docking procedure.[19] The authors proposed that the dimer would be disrupted upon translocation and autophosphorylation, leading to an active PDK1 monomer.

The first crystal structure of the human PDK1 kinase domain cocrystallized with an ATP molecule was released in 2003 (PDB ID 1H1W). The structure defined the presence of a hydrophobic pocket, denominated the PIF-pocket, within the small lobe of the PDK1 catalytic domain, which was meant to be required for the binding of PDK1 to the hydrophobic motif of its substrates; an adjacent phosphate-binding site was also revealed.[20] The most recent human PDK1 KD crystallographic structure in complex with a peptide bound to the PIF-pocket was launched in 2016.[21] In that study, the authors described the allosteric connection between the ATP-binding site and the PIF-pocket, which was modulated by small compounds bound to the active site. Additionally, molecular dynamics simulations of the KD showed that there was a dynamic equilibrium between the open and closed conformations of the KD domain and validated the key roles of Lys144 and Lys199 in stabilizing the closed-active and open-inactive forms of the kinase, respectively.[21] Crystallographic structures of the uncomplexed PDK1 PH domain (PDB ID 1W1H), the PDK1 PH domain complexed with PIP3 (PDB ID 1W1G), and the PDK1 PH domain complexed with inositol (1,3,4,5)-tetrakisphosphate (Ins(1,3,4,5)P4, PIP4) (PDB ID 1W1D) were launched in 2004, which revealed significant differences compared to standard PH folds.[22] Thus, the PDK1 PH domain shows a N-terminal extension of two extra antiparallel β-sheets and an extra α-helix, which create a new hydrophobic core. Moreover, the PDK1 PH domain possesses a much more spacious ligand-binding site. As in other PH domains, the PDK1 PH domain is bound to the phosphate groups of phosphoinositides at the plasma membrane by several positive residues (Arg472, Arg474, Arg521, Lys465, and Lys467, among others) lined along the VL1−3 loops. Using a qualitative protein−phospholipid overlay assay, it was observed that the mutant PDK1(mutated K465E) failed to bind phosphoinositides. The explanation is that residue Lys465 forms key hydrogen bonds with the D3 and D4 phosphates of PIP3, which are lost in the K465E mutant.[22] Using a time-resolved fluorescence resonance energy transfer assay, it was also detected that PDK1(mutated K467A) interacted with all D5-phosphorylated inositides with a lower affinity. Additionally, the overlay of the uncomplexed PDK1 PH domain structure with the structures of the PDK1 PH−PIP3 and PH−PIP4 complexes indicate that the PH domain does not undergo a conformational change when it binds to phosphoinositides, as suggested previously.

The role of the PDK1 PH domain in the activation of PKB was then analyzed by knock-in mutation. First, knock-in PDK1(mutated LLL) embryonic stem cells were generated by mutating Arg472, Arg473, and Arg474 to three Leu groups.[23] It was observed that the lack of interaction of PDK1 with the membrane resulted in reduced PKB activation, but PDK1 expression levels were also reduced. However, further research could not be done because the PDK1(mutated LLL) knock-in mice died at embryonic age. The 1W1G structure of the PDK1 PH−PIP3 complex revealed that the Arg473L mutation could cause PH domain instability, leading to hypomorphic expression levels of the mutant protein that could in turn cause the lethal phenotypes.

To validate the mechanism for the activation of PKB by PDK1 and at the same time generate new tools to manipulate PKB activation, a rationally designed structural-based point mutation was engineered to replace Lys465 within the PDK1 PH domain with Glu. While the overall folding of the PDK1−PH(mutant K465E) crystal (PDB ID 2VKI) was preserved, thereby accounting for the stability of the mutated PH domain, the positions of the charged side chains of close residues lined at the PH−membrane interface were different and, consequently, the positive charge of the PtdIns(3,4,5)P_3 binding site was severely reduced.[24]

Functional analysis of the PDK1 K465E mutation was next addressed in vivo by generating knock-in mice physiologically expressed from the endogenous locus of the mutant rather than the wild-type version of PDK1. Since the anticipated lack of activation of PKB could have led to embryonic lethality, the expression of the PDK1 K465E protein was circumscribed to muscle tissues using Cre-Lox methodologies.[5,25] In contrast to PDK1(mutated LLL), the PDK1 K465E mutation did not compromise PDK1 expression levels. Puzzlingly, it was previously found that the activation of PKB by insulin administration was selectively, albeit only modestly, diminished but not abolished in muscle protein extracts of the mutant mice when compared to the wild-type controls (Bayascas and Alessi, unpublished data). To rule out whether the observed PKB activation reflected the partial penetration of the mutation into the skeletal muscle, full-body knock-in mice were then generated, which were viable, smaller in size, and exhibited no overt phenotypes. In tissues derived from these mice, a partial rather than total ablation of PKB activation was confirmed, although the PDK1 K465E mutant protein was incapable of PtdIns(3,4,5)P_3 binding in vivo.[24]

The finding that PDK1(mutated K465E) was still able to activate PKB suggested that there was another mechanism for the phosphorylation of PKB that was independent of PtdIns(3,4,5)P_3 binding. Although the insulin-like growth factor 1 (IGF1) induced recruitment of the isolated PDK1 PH domain to the plasma membrane was avoided in cells with the K465E mutation, the dynamic translocation of the isolated PH domains was found to function differently from that of full-

https://doi.org/10.1021/acsomega.2c02020
ACS Omega 2022, 7, 25186−25199

length PDK1; indeed, PDK1 was mainly cytosolic, with only a small fraction present at the membrane, and did not markedly translocate to the plasma membrane following the stimulation of cells with IGF1.[22] A pool of full-length PDK1 was previously noticed to be located at the plasma membrane in resting cells, which in contrast to PKB was not further enriched by growth factors.[11] This PtdIns(3,4,5)P_3-independent plasma membrane localization most likely relies on binding to other anionic phospholipids such as phosphatidylserine.[26,27] Additionally, the kinase domain of PDK1 has been shown to play a prominent role in PDK1 membrane localization.[28] Once at the membrane, the prior phosphorylation of the PKB hydrophobic motif at Ser473 by mTORC2 may drive the docking of the PDK1 K465E protein to the PIF-pocket, allowing the phosphorylation and activation of PKB by PDK1, albeit to lower levels.[29,30]

Although subtle, this signaling lesion resulted in knock-in male and female mice smaller than those that presented insulin resistance[24] and neuronal dysfunctions.[29,31,32] More recently, behavioral analysis of the PDK1(mutated K465E) knock-in mice has enhanced the relevance of this mutation, which fine-tunes the regulatory mechanism of PKB activation and leads to several physiological responses in vivo that are sex-, age-, and genetic load-dependent.[33,34]

To gain insights into the mechanism of regulation of PDK1, we aimed to understand how the PDK1 K465E mutant kinase could still activate PKB in the absence of phosphoinositide binding. To that end, docking and molecular dynamics (MD) calculations were performed for the first time to model and simulate the wild-type KD−PH and the KD−PH(mutant K465E) PDK1 complexes. The same analyses were performed with PH-in and a PH-out conformations of wild-type PDK1 and a PH-in model of KD−PH(mutant K465E) PDK1. In addition, three KD−PH complexes were simulated, including a substrate analogue bound to the PIF-pocket. By comparing the different in silico KD−PH complexes, we found that only the PH-out conformation was active for the wild-type PDK1, whereas the active conformation of the PDK1 K465E mutant was PH-in, since the ATP remained stable at the active site while the PIF-pocket was more accessible to the peptide substrate. We corroborate that both the docking-site binding and the catalytic activity were in fact enhanced in the PDK1 K465E protein compared to the wild-type, even in unstimulated cells. Introducing the K465E amino acid substitution in the K465E PH-in conformer might have evoked the Thr513 phosphorylation-mediated PDK1 activation mechanism;[18] indeed, both glutamate substitution and phosphorylation resulted in the incorporation of additional negative charges into the VL-loop region, improving the PH-in conformation and leading to the enhanced activation of the enzyme.

2. SIMULATED MODELS

2.1. Models of the PH and KD Domains. In this work, we built several models of the KD−PH complex. In all cases, the initial coordinates for the PH domain were taken from the crystallographic structure with PDB ID 1W1H.[22] For the KD domain, we used two different sets of coordinates corresponding to PDB IDs 1H1W and 5LVP.[20,21] In both cases, there are missing residues that belong to the activation loop (residues 233−236 in 1H1W and residues 231−239 in 5LVP). These were modeled with the program MODELER[35,36] using the 3HRF structure as a template for the missing segment.[37] The resulting structures were used to build the model of the KD domain with residue Ser241 of the activation loop phosphorylated. In the 5LVP structure, PDK1(50−359) was cocrystallized in the presence of the phosphorylated peptide KGAGGGGFPQFS(P)YSA (underlined residues were conserved in the hydrophobic motif (HM) of Akts or PKBs, SGKs, S6Ks, and PKCs). Thus, in our second KD model, we have included the HM-phosphorylated peptide sequence FPQFS(P)YS.

Hydrogen atoms were added with the module HBUILD from the program CHARMM,[38,39] and the protonation states of the titrable residues were determined with the PROPKA algorithm.[40] In accordance with the high pK_a (8.5) calculated by PROPKA, the residue Glu188 was protonated in the 5LVP model. The modeled fragment was first minimized by 100 steps with the adopted basis Newton−Raphson (ABNR) method of the program CHARMM,[38] then 100 steps of ABNR minimization were performed on the side chains of all the residues in the KD domain. These minimizations were done in the presence of the crystallographic waters.

The same protocol was used to obtain a model of the PH domain that included polar hydrogens and the side chains of all the residues in optimized positions.

2.2. Models of the KD−PH Complex. *2.2.1. Complex KD(1H1W)−PH(Wild-Type)-In.* The KD model built from the 1H1W structure (as described above) was docked with the PH model (described above) to generate representative structures of the KD−KD complex. The docking was performed in the absence of water molecules with the program ZDOCK.[41] ZDOCK performs global searches were one of the molecules is fixed (the KD domain in our case) and the other is docked in different positions (PH domain). The results are filtered such that only those with specified residues (defined by the user) in the binding site are returned. From the 2000 structures generated, only 13 structures accomplished the restriction that was used in this work to define the PH-in conformation, that is, that all the PIF-pocket residues of the KD and the Lys465 of the PH domain were in the binding region simultaneously. These 13 structures were re-ranked with the ZRANK program[42] (after hydrogen atoms were added to the ZDOCK generated files), and the lowest-energy structure was selected as the input of the ROSIE server.[43] The RosettaDock Server performs a *local* docking search. That is, the algorithm will search a set of conformations *near the given starting conformation* for the optimal fit between the two partners. We used the Docking 2 protocol. From the structures created in the docking run, we selected the one with lowest interface energy. This final structure was used to perform 780 ns MD simulations with the program AMBER,[44,45] (see section 3). In these simulations, the ATP molecule was added to the KD domain using the original crystallographic coordinates. This model is a representation of the wild-type KD−PH interaction in the PH-in configuration.

2.2.2. Complex KD(1H1W)−PH(Mutant K465E)-In. We started from the complex KD(1H1W)−PH(wild-type)-in by mutating the residue Lys465 to a Glu residue with the VMD program.[46] We then added the original ATP coordinates. After a first period of minimization and equilibration, we performed 780 ns MD simulations with the program AMBER (see section 3). This model is a representation of the KD−PH(mutant K465E) interaction in the PH-in configuration.

2.2.3. Complex KD(1H1W)−PH(Wild-Type)-Out. To generate a representative structure of the wild-type KD−PH interaction in the PH-out configuration, a docking procedure

https://doi.org/10.1021/acsomega.2c02020
ACS Omega 2022, 7, 25186−25199

was followed with the ZDOCK program without using any restrictions or blocking residues. The ten lowest-energy structures generated by the program were re-ranked. Representative configurations of the PH-out state were selected using the following criteria: (1) a distance larger than 25 Å between the residue Leu155 of the PIF-pocket and the residue Lys465 of the VL1-loop and (2) the VL-loops should be rotated out of the protein surface region and back to the PIF-pocket. Under these criteria, only 2 of the 10 lowest-energy structures mentioned above presented a PH-out configuration, and the one with the lowest energy was chosen as the input of the RosettaDock server to follow the same docking protocol and MD procedure mentioned in section 2.2.1 (with the ATP molecule included in the MD simulations).

2.2.4. Models from 5LVP the Crystallographic Structure: KD−PH(Wild-Type)-In, KD−PH(Mutant)-In, and KD−PH-(Wild-Type)-Out Models with the HM-Phosphorylated Peptide Sequence in the PIF Pocket. With the most recent X-ray crystallographic structure, we followed a slightly different strategy to obtain the models of the KD−PH wild-type or mutant complexes in the two different configurations that included the HM peptide. The KD model built from the 5LVP structure (as described above) was docked, without using any restrictions or blocking residues, with the PH model (described above) to generate representative structures of the KD−PH complex.

Among the ten most-stable structures (re-ranked by the ZRANK program), we selected one that was more representative of the PH-in configuration (that is, with the VL-loops rotated toward the internal zone of the complex, facing the PIF pocked and the helix-αC) and another representative of the PH-out configuration (under the criteria described above). Both structures were refined with the RosettaDock Server. The lowest-interface-energy structures were selected for both the in and out configurations and completed with the ATP molecule in its X-ray position in the KD domain before a long MD simulation was initialized to study the stability and behavior of the ternary complexes in the two different PH configurations (in and out).

In addition, the mutant KD−PH-in model was built from the initial wild-type KD−PH-in model complex by mutating the residue Lys465 to a Glu residue with the VMD program.[46] Next, a MD simulation was carried out for this model, similar to that for the mutant complex built from the 1H1W structure.

3. SIMULATION PROTOCOL

Each model was solvated with a nearly cubic pre-equilibrated box of TIP3P[47] water molecules (of dimensions around 194 Å × 185 Å × 180 Å). The final solvated models had around 100 000 atoms each. A buffering distance of 12 Å was established between the atoms of the enzyme and the edge of the box. Water molecules closer than 1.0 Å to any atom of the ligands or the enzyme were removed. The total charge of the system was neutralized by including one Cl^- ion or one Na^+ ion depending on the model. The AMBER ff14SB[48] force field was employed to define the protein residues, and the phossaa10[49] force field was used to define the molecular mechanics (MM) parameters of the ATP phosphate groups.

The following simulation protocol was used for all the models:

1. Two hundred energy minimization steps, with restraints applied on the Cartesian coordinates of the protein domains and ligands (ATP and HM-peptide).
2. Two hundred energy minimization steps for the entire molecular system.
3. Periodic boundary MD simulations at constant volume were performed for 10 ps of heating up to 300 K, followed by 110 ps of equilibration through periodic boundary MD simulations at constant temperature and pressure. The weak-coupling algorithm and the Berendsen barostat[50] were employed for temperature and pressure regulation, respectively. The SHAKE algorithm[51] was applied to constrain bond distances involving H atoms.
4. Particle mesh Ewald molecular dynamics (PMEMD)[52,53] simulations to reach 780 ns. Along the production period under periodic boundary conditions, the temperature was controlled by Langevin dynamics[54] and the pressure was regulated by the Berendsen barostat. No restraints were applied besides those imposed by the SHAKE algorithm.

   A time-step of 2 fs was used for the MD trajectories. The minimization, heating, and equilibration steps (1−3 above) were performed with the SANDER module of the AMBER 14 program.[44] The production stage was carried out with the AMBER 16 GPU (CUDA) version of the PMEMD package.[55,56]

We analyzed the trajectories generated for the six models of the KD−PH complex in different configurations using the program CPPTRAJ (C++ Process Trajectory). In all cases, we used the *rmsd* command to perform RMSD calculations and the *hbond* and *distance* commands to analyze inter atomic interactions between parts of the system. During the simulation, the trajectory was saved every 5000 steps, that is, every 10 ps, for analysis.

4. RESULTS AND DISCUSSION

We first sought to biochemically determine the subcellular localization of PDK1 to clarify whether agonist stimulation, PtdIns(3,4,5)P_3 production, or phosphoinositide binding dynamically relocated PDK1 pools. To that end, cytosolic and membrane protein fractions obtained from muscle tissue extracts derived from PDK1 K465E mutant and PDK1 wild-type control littermate mice, who were or were not injected with insulin, were analyzed by Western blot. As depicted in Figure 1, PDK1 is mainly cytosolic in the unstimulated control tissues, and only a small proportion of the total protein was detected in the membrane fractions in both the wild-type and mutant samples. In contrast to the PKB kinase, which is excluded from the membrane in resting conditions and enriched in these fractions by insulin in both control and mutant tissues, membrane-associated levels of PDK1 are neither further increased by insulin in wild-type or mutant samples not excluded from the membrane in the mutant samples by the PDK1 K465E mutation. Therefore, a pool of PDK1 protein constitutively associated with membranes in an agonist-independent manner is definitively demonstrated; this is preserved in the PDK1 K465E samples, thereby evidencing the participation of other mechanisms, such as the suggested phosphatidylserine binding site or the kinase domain, in anchoring PDK1 to the plasma membrane.[27,28]

https://doi.org/10.1021/acsomega.2c02020
ACS Omega 2022, 7, 25186−25199

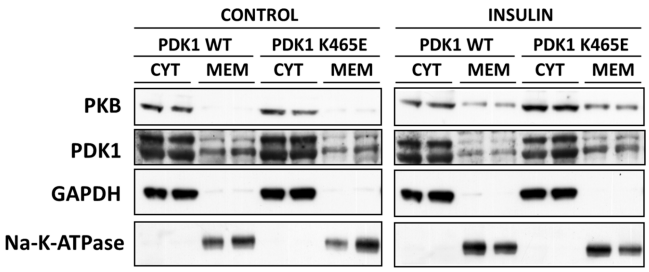

Figure 1. Subcellular localization of endogenous PDK1. Mice were fasted overnight and intravenously injected with either saline (CONTROL) or 0.5 mU/g insulin (INSULIN). Protein extracts were obtained from knock-in mutant (PDK1 K465E) and control wild-type (PDK1 wild-type) muscle tissues, which were fractionated into cytosolic (CYT) and membrane (MEM) fractions. Samples were subsequently analyzed by Western blot with PKB, PDK1, the cytosolic marker GAPDH, and the plasma membrane marker Na-K-ATPase antibodies. The results are representative of three experiments, where each lane represents a sample derived from a different mouse.

This PDK1 K465E enzyme anchored to the membrane in a PtdIns(3,4,5)P_3-independent manner has been widely shown to be unproficient at phosphorylating PKB.[23,29] The surfing of membrane-bound wild-type PDK1 to PtdIns(3,4,5)P_3-enriched rafts, where PKB will be expected to be located upon agonist stimulation, could account for normal PKB activation, which will be prevented in the mutant samples. Yet, in the PDK1 K465E mice, the considerable activation of PKB was still observed. We hypothesize that changing Lys at the critical position 465 into Glu may have structural and functional consequences for PDK1 regulation beyond preventing PtdIns(3,4,5)P_3 binding, which could explain the remaining PKB activation in the mutant tissues. To explore that possibility, docking and molecular dynamics calculations of the wild-type KD−PH and the mutant KD−PH(K465E) PDK1 complexes were modeled as described in section 3. In all the six models constructed, the RMSD calculation (Figure S1) shows that the complex system has stable dynamical behavior. The PH domain is more mobile than the KD domain in all cases. Visual inspection of the trajectories indicates that the two domains, KD and PH, interact all along the simulations and that the complex rotates as a whole.

In the analysis of the trajectories generated for each of the models, we focused our attention on interactions or conformational changes related to key residues of the enzymatic system whose roles in catalysis or kinase activation have been proposed in the literature. In particular,

1. The dynamical behavior of ATP in the active site and its interactions with the conserved residue Lys111 or others.
2. The salt bridge between Lys111 and Glu130, a highly conserved salt bridge between a Lys that positions the phosphate of ATP at the active site and a Glu from helix-αC (Lys111 and Glu130 in PDK1), because it is widely considered a hallmark of active structures of protein kinases.[20,57]
3. The salt bridge formed by Lys144 and Asp138, which was experimentally observed only in the closed form of the complex and not in the open form, where it was replaced by the Lys199-Asp138 interaction.
4. The distance between the conserved PH residue K465 (or, when mutated in the mutant models, E465) and the PIF-pocket (residues Lys115, Ile118, and Ile119 in the αB-helix; residues Val124 and Val127 in the αC-helix; and residue Leu155 in β-sheet5).

Figure 2a shows the relative positions of the above-mentioned residues in the initial structure of the complex KD(1H1W)−PH(wild-type)-in. Lys111 is located between the PIF-pocket (around 8−10 Å from it) and the ATP molecule. It interacts with the ATP phosphate arm and the residue Glu130 (represented in Figure 2a but not in Figure 2b) simultaneously through salt-bridge interactions. The Asp138 residue is located

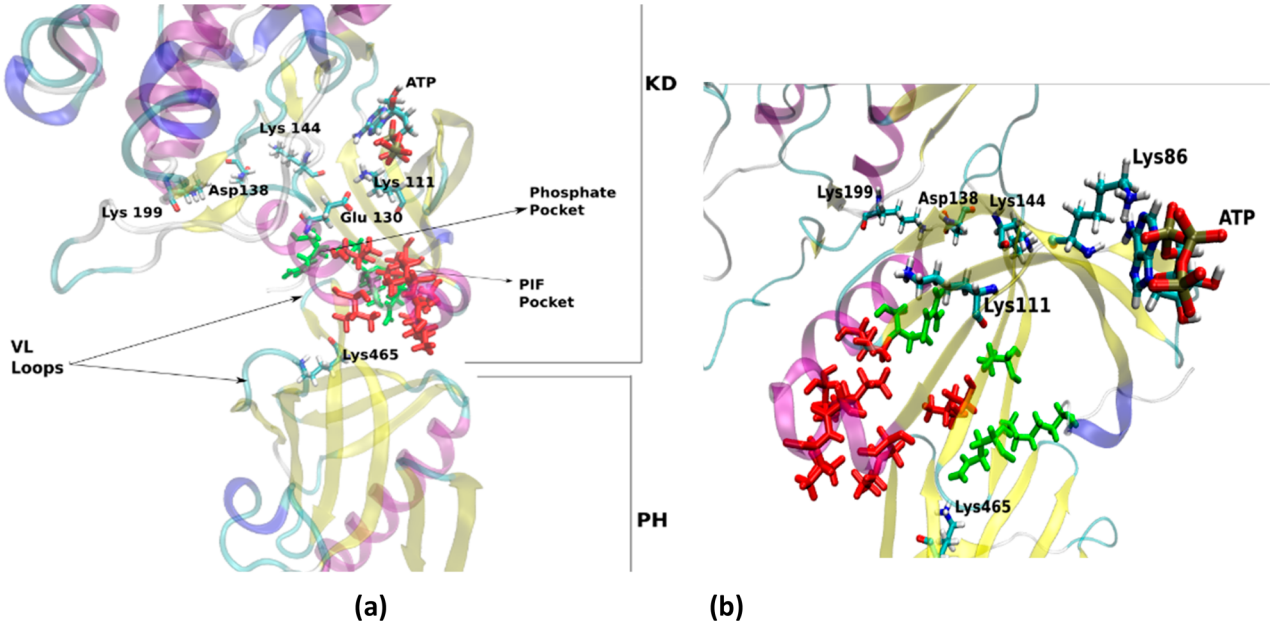

Figure 2. (a) Initial KD(1H1W)−PH(wild-type)-in model. The side chains of relevant kinase residues are represented in sticks and colored by atom type. The residues shown as green and red sticks correspond to the phosphate pocket and the PIF-pocket, respectively. (b) Final structure from the MD simulation of the KD(1H1W)−PH(wild-type)-in complex. See panel a for the meanings of the colors used.

https://doi.org/10.1021/acsomega.2c02020
ACS Omega 2022, 7, 25186−25199

between the two lysine residues, namely, Lys144 and Lys199, in an intermediate position (neither the closed nor open configuration). The VL-loops are formed by positively charge residues (Lys465, Arg472, Lys512, etc.) that interact with negatively charged residues of the small lobe of the KD domain (for example, Asp132 and Glu153).

Figure 3a shows the movement of ATP from its initial interaction with Lys111. The ATP molecule goes far from the

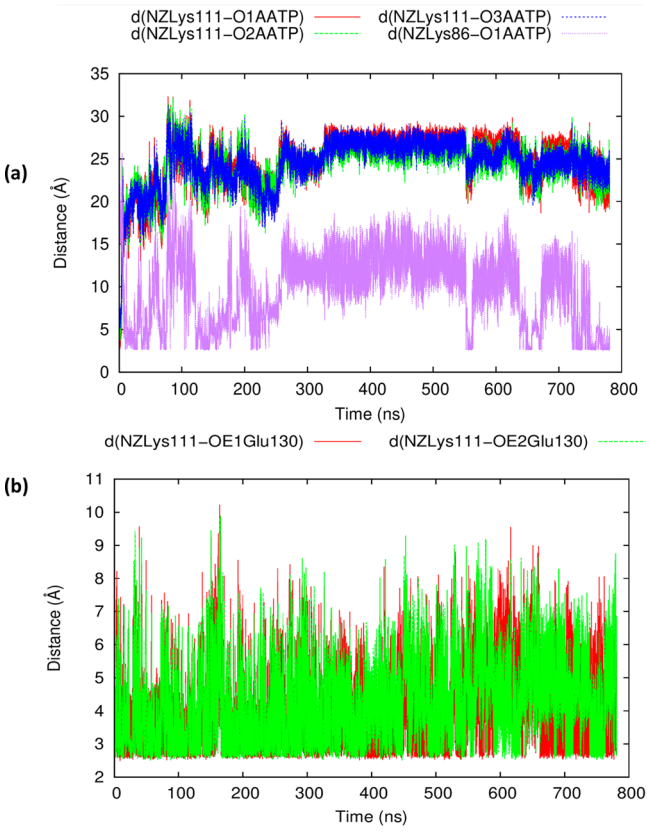

Figure 3. The KD(1H1W)−PH(wild-type)-in complex. (a) Distances between Lys111 or Lys86 and ATP. (b) The salt bridge between Lys111 and Glu130.

active site to interact with Lys86, whose position in the protein complex can be seen in Figure 2b. Figure 3b indicates that the salt-bridge interactions between the conserved residues Lys111 and Glu130 do not significantly change despite the ATP movement. Figure S2a compares the RMSDs of ATP, which were calculated with the first structure or the average structure as references, respectively, revealing that the ATP movement occurs at the very beginning of the simulation. The analysis of the structures along the trajectory shows that at the beginning of the simulation Glu130 simultaneously interacts with the adenine ring of the ATP molecules (N6 atom), the NH_3^+ side-chain of Lys111, and the −NH main-chain groups of residues Gly225 and Phe224 located in a loop nearby the activation loop. Another negative side-chain residue in the same loop, Asp223, approaches Lys111 (the distance between them is reduced by 3 Å along the first quarter of the trajectory) and anchors it near Glu130. The stability of the Asp223−Lys111 and Glu130−Lys111 interactions is supported by residence times of 28.92% and 37.07%, respectively, as indicated in Table S1 of the Supporting Information file. This seems to be the main reason why Lys111 loses its initial interaction with the α-phosphate group of ATP (with only 0.09% of the residence time), whereas at the beginning of the simulation it competes with Glu130 and Asp223 in their interactions with Lys111. Finally, the interaction of the O1A atom of ATP with the NZ atom of Lys111 is lost, and ATP moves away to find other interactions, as shown in the final structures of the simulation.

Regarding the dynamics of the protein, at the start of the simulation, the Asp138 residue interacts with Lys144. However, after approximately 80 ns, it rotates to interact with Lys199, thus going from the closed form to the open form (see Figure S3a). During the simulation, the distance between the geometric center of the PIF-pocket residues and the geometric center of a group of four VL-1 residues around Lys465 (residues 463−466) increases from 12−14 Å to 16−18 Å (Figure S4a).

When the simulation is carried out with the mutant model complex (complex KD(1H1W)−PH(mutant K465E)-in), the ATP molecule remains at the same position in the active site for the first quarter of the simulation, as can be seen in Figure 4a. After that, it moves to interact with positively charged

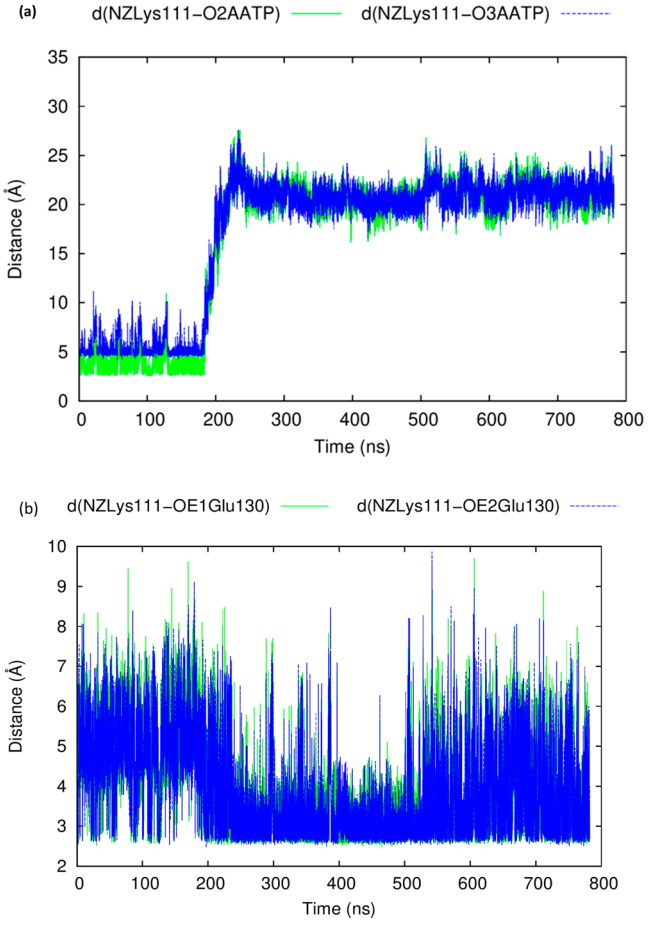

Figure 4. The KD(1H1W)−PH(mutant K465E)-in complex. (a) Distances between Lys111 and ATP. (b) The salt bridge between Lys111 and Glu130.

residues of the activation loop (Arg238 and Lys235) and a positively charged residue in the VL loop (Lys512). The movement of ATP far from Lys111 correlates with a strengthening of the Lys111−Glu130 interaction (as seen in Figure 4b). It is interesting to observe that there is a clearer oscillation of the enzymatic system between the open and

https://doi.org/10.1021/acsomega.2c02020
ACS Omega 2022, 7, 25186−25199

closed forms during the time ATP and Lys111 maintain their interaction, as shown in Figure S3b. After that, the system dynamics stabilize the open-form configuration.

For the mutant model, the distance between the PIF residues and the VL-1 residues is slightly shorter (11−16 Å) than the corresponding one in the wild-type model (Figure S4b).

Figure 5 shows the relative positions of the key residues mentioned above at the end of the complex KD(1H1W)−PH(mutant K465E)-in simulation.

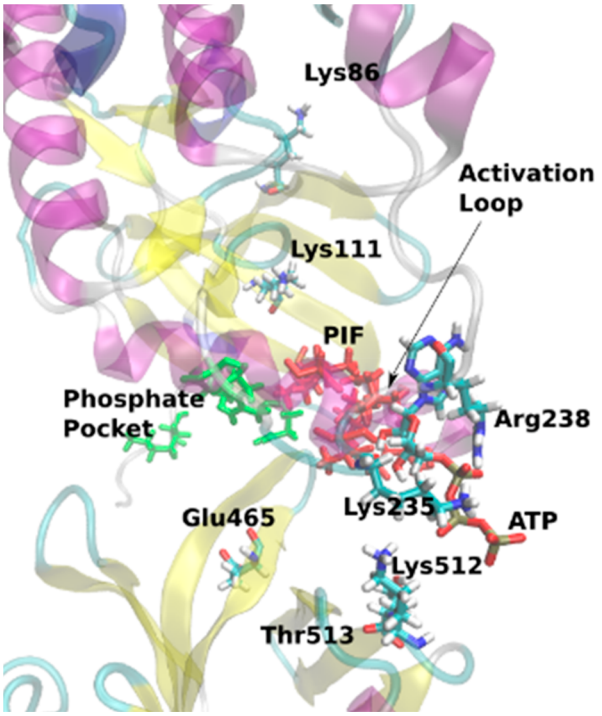

Figure 5. Final structure of the KD(1H1W)−PH(mutant K465E)-in complex from the MD simulation. See Figure 2 for the meanings of the colors used.

The results obtained for the third model built from the 1H1W structure, namely, complex KD(1H1W)−PH(wild-type)-out where the interaction between the KD and the PH domain is not though the VL-loops but instead between the large lobe of the KD domain and the helices of the PH domain (see Figure 6a), indicate that the ATP molecule maintains its position in the active site for the entire simulation (Figure 7a). this might be correlated with the fact that the distance between Glu130 and Lys111 is larger than those in the previous models (see Figure 7b), as the interaction between Lys111 and ATP weakens the Lys−Glu salt-bridge. The analysis of the interactions established by Glu130 along the MD trajectory suggests that this residue, together with the loop formed by residues Gly225 and Phe224, which are hydrogen-bonded to Glu130 (as seen in the wild-type and mutant PH-in model complexes), has enough space to move away from the Lys111−ATP dyad. Finally, Glu130 interacts with another positive residue, Arg131, as seen from the snapshot at around 650 ns. The residence time of this interaction is 38.15% (see Table S1). This new interaction is established as an alternative to the salt bridge with Lys111, which now anchors the ATP molecule in the active site with a residence time of 70.08%.

Figure 6b shows the relative positions of the key residues at the end of the simulation, showing that they do not significantly change from the beginning of the simulation and thus supporting the stabilization of the system in the PH-out configuration with the ATP molecule within the active site. Interestingly, Asp138, which also changes its interaction with Lys144 by interacting with Lys199 as in the PH-in configuration, is more mobile in this PH-out model, as seen when comparing Figure S3a and c in the Supporting Information file.

The KD(1H1W)−PH(mutant K465E)-out complex was not modeled because the PH-out conformation with the PH domain well-oriented to interact with the cellular membrane could never be stabilized in the mutant, as unfavorable electrostatic interactions with PtdIns(3,4,5)P_3 prevented binding.

The results obtained for the models built from the 5LVP X-ray structure of the KD domain shed light on the effect of the substrate in the active site. Figure 8a shows the initial disposition of the key residues of the system at the beginning of the simulation for the model KD(5LVP)−PH(wild-type)-in. The position of the HM-peptide substrate (in gray) that interacts with the PIF-pocket residues is shown.

As occurred for the model built from the 1H1W structure, in the case of the PH-in configuration of the wild-type complex, the ATP molecule migrates to interact to other positively charged residues other than Lys111. However, in this case, instead of forming interactions with KD residues, it is the VL-loop residue Lys465 that mainly stabilizes the final position of the ATP molecule (see Figure 8b). A general difference between the PH-in structures generated from 5LVP and those generated from 1H1W is the larger distance in the former (23−30 Å in comparison to 12−18 Å) between the PIF-pocket and the VL-loops (see Figure S4d), what may explain the different behavior of ATP.

In addition, that larger difference in the VL-loops−PIF distance, the presence of the substrate, and perhaps other causes that we have not been able to detect result in the stabilization of the ATP molecule in the active site of the mutant model complex KD(5LVP)−PH(K465E)-in. Figure 9a shows that ATP interacts with Lys111 all along the simulation. That interaction, with a residence time of 95.55%, is correlated with a weaker interaction of the salt bridge Lys111−Glu130 (Figure 9b) and a clearer oscillation of the system between the open and closed forms (Asp138 alternatively interacts with Lys144 and Lys199 along the simulation, Figure 9c). It is worth noting that, as seen in the previous models, Glu130 establishes hydrogen-bond interactions with the main-chain −NH groups of residues 223−225 (see the larger residence time interaction values of 61.63% and 25.36% for this model in Table S1) and is closer to the αC-helix. Therefore, the mutation in the VL-loops in the presence of the substrate seems to widen the space between the 130−223−225-αC-helix region and the Lys−ATP dyad, thus contributing to reinforcing the interactions between the latter two residues. The larger separation between Glu130 and the Lys111−ATP dyad explains the stability of ATP in the active site and seems to be correlated with the oscillation between the open and closed forms of the KD domain, which is associated with the active state of the enzyme, as mentioned in the literature. This active state is reached when ATP and then the substrate have entered in the active site but not in the absence of the substrate, as

https://doi.org/10.1021/acsomega.2c02020
ACS Omega 2022, 7, 25186−25199

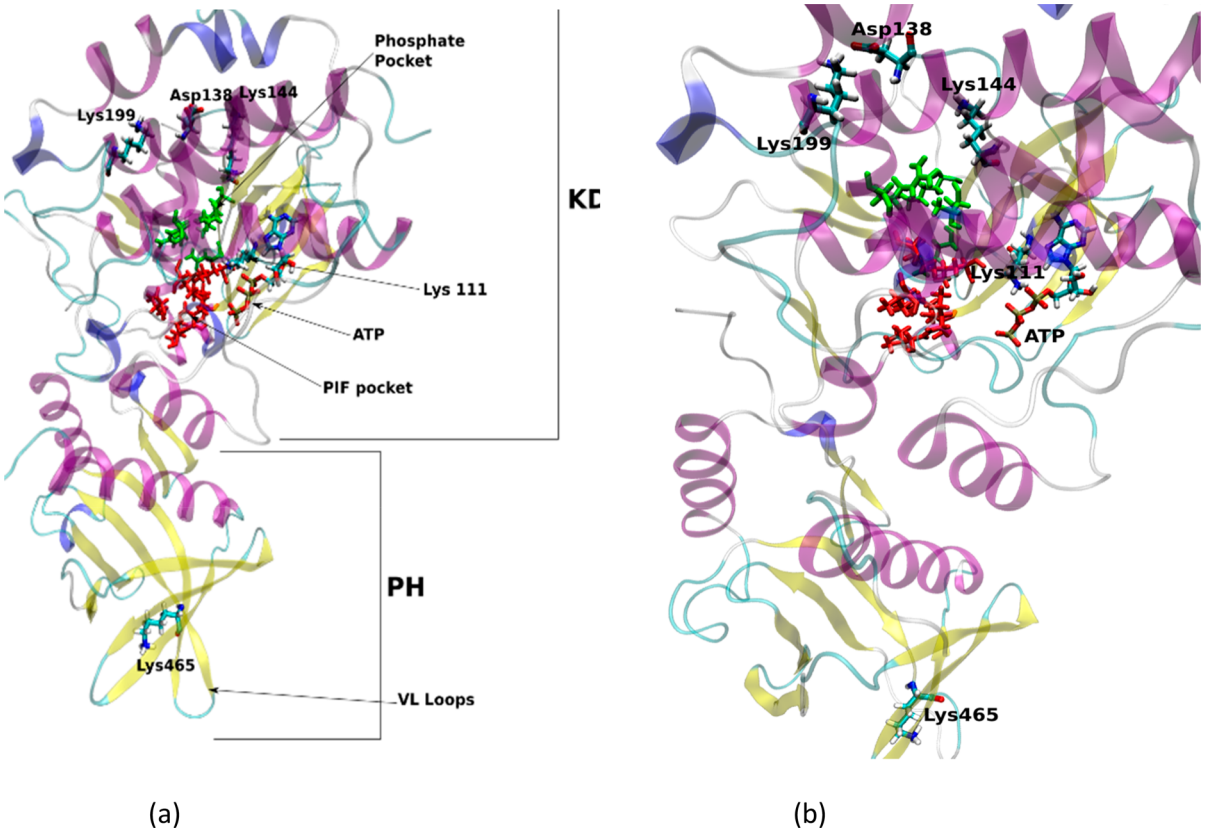

Figure 6. (a) Initial structure of the KD(1H1W)−PH(wild-type)-out complex from the MD simulation. See Figure 2 for the meanings of the colors used. (b) Final structure of the KD(1H1W)−PH(wild-type)-out complex from the MD simulation. See Figure 2 for the meanings of the colors used.

suggested by the negative (no oscillation) result obtained for our theoretical models without the substrate.

Figure 10 shows the final positions of the key residues in the active site at the end of the simulation. The data collected in Table S1 of the Supporting Information file reinforce the idea that the mutant model KD(5LVP)−PH(K465E)-in is closer to the out conformation of the KD(5LVP)−PH(wild-type)-out complex (see below) than to the in conformation of the KD(5VLP)−PH(wild-type)-in complex.

Finally, the results obtained for the model built from the 5LVP structure representing the PH-out configuration, namely KD(5LVP)−PH(wild-type)-out, indicate that the PH-out configuration of the system also maintains the ATP ligand in the active site in the presence of the HM-peptide substrate. This is shown by the analysis of the trajectory (see Figure 11), which goes from the initial configuration represented in Figure 12a to the final snapshot represented in Figure 12b.

Interestingly, the structures generated with this model in the PH-out configuration, the substrate HM-peptide, and the ATP ligands in the active site clearly oscillate between the open and closed forms of the KD domain (see Figure 13), and a looser salt-bridge interaction between Lys111 and Glu130 is present (see Figure 14). That result supports an equilibrium between the open and closed conformations of PDK1, as proposed previously.[21]

In the PDK1 K465E protein, molecular modeling data suggested that replacing lysine at position 465 with glutamate resulted in the stabilization of the ATP molecule at the active site. This was accompanied by a clear oscillation between open and closed forms, as revealed by Asp138 residue alternatively interacting with Lys144 and Lys199 along the simulation. These changes may have promoted a partial transition of the mutant PDK1 enzyme to the out conformation, analogous to that induced by the binding of the wild-type PH domain to PIP3 but less efficient. This conformation may have enabled PDK1 K465E to dock to the phosphorylated hydrophobic motif of membrane-located PKB,[58] allowing Thr308 phosphorylation. To test these predictions, a peptide encompassing the hydrophobic motif sequence of the PKC-related protein kinase 2 (PRK2), termed PIF-tide (from PDK1 interacting fragment peptide) was employed to perform the affinity purification of PDK1 from protein extracts derived from PDK1 wild-type and PDK1 mutant mouse tissues. As shown in Figure 15, the interaction of PDK1 with the docking-site-emulating peptide was enhanced by the PDK1 K465E mutation in most tissues analyzed. By contrast, PDK1 was purified with PIF-sepharose from liver protein extracts derived from PDK1 wild-type and PDK1 K465E knock-in mice with the same efficiency, an unexplained tissue singularity that was observed previously.[24]

Moreover, the catalytic activity of PDK1 immunoprecipitated from wild-type and mutant mouse muscle samples was assayed in vitro against two different peptides, the T308tide corresponding to the T-loop of PKB, and the PDKtide, which consisted of both the sequence of the T308tide and the sequence of the PIFtide. As shown in Figure 16, the catalytic activity of PDK1 against the T308tide is similar in the wild-type and the mutant samples and is not enhanced by insulin administration, thereby supporting the notion of PDK1 as a constitutively active enzyme. As reported previously, the

https://doi.org/10.1021/acsomega.2c02020
ACS Omega 2022, 7, 25186−25199

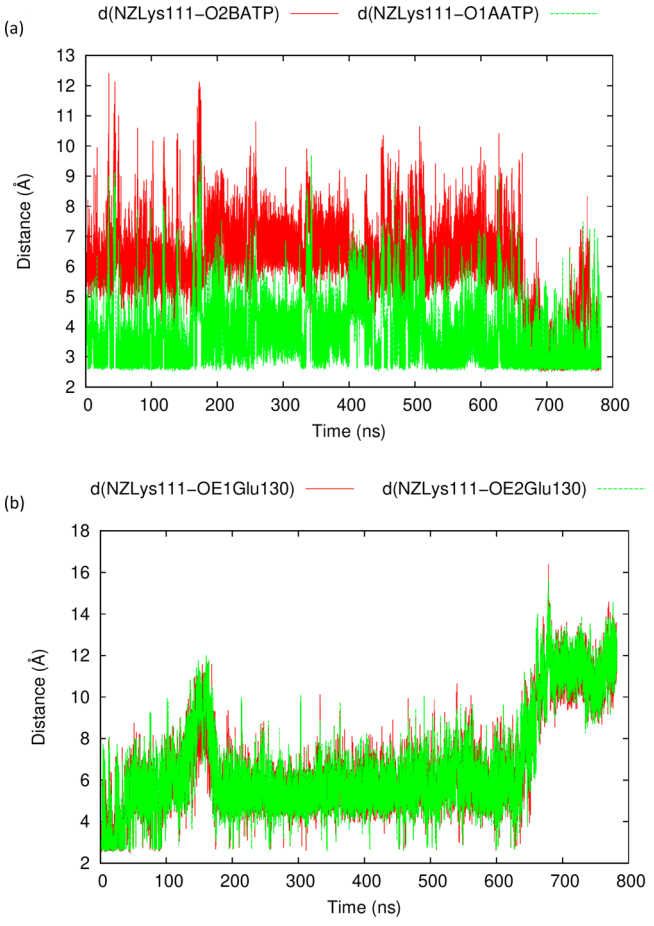

Figure 7. The KD(1H1W)−PH(wild-type)-out complex. (a) Distances between Lys111 and ATP. (b) Thee salt bridge between Lys111 and Glu130.

presence of a docking site sequence next to the T-loop in PDKtide enhances the PDK1 activity, which is not further increased by insulin, twofold in the wild-type samples. Of note, in the PDK1 K465E samples, the PDK1 activity against PDK1tide was found to be induced threefold compared to that in the T308 assay, thereby demonstrated that the improved binding of the PDK1 K465E mutant protein to the substrate-docking site might have been sufficient to enable the phosphorylation of PKB in the mutant mouse samples even in the absence of PtdIns(3,4,5)P_3 binding.

5. CONCLUSIONS

In summary, the results presented here for the PDK1 wild-type enzyme in the PH-in configuration are coherent with the generally accepted idea that one of the factors regulating PDK1 activity is its change to a configuration where the VL-loops of the PH domain do not face the PIF-pocket but are oriented in an opposite direction toward the external face of the KD−PH complex (PH-out configuration), which is triggered by the interaction with the PtdIns(3,4,5)P_3 lipid at the cellular membrane. This is supported by the fact that in our PH-out models (KD(1H1W)−PH(wild-type)-out and KD(5LVP)−PH(wild-type)-out) the ATP molecule is stable in the active site independent of the presence or absence of the HM of the substrate in the active site, whereas the PH-in modeled configurations (KD(1H1W)−PH(wild-type)-in and KD-(5LVP)−PH(wild-type)-in) are not able to maintain the reactive disposition of the ATP ligand. Importantly, the results obtained for the simulated K465E mutation (complexes KD(1H1W)−PH (mutant K465E)-in and KD(5LVP)−PH-(K465E)-in) suggest that the PH-in configuration of the mutant might be partially active, as ATP is maintained in the active site, especially in the presence of the HM of the substrate. The presence of the negatively charge amino acid Glu rather than the positively charge Lys at position 465 could have promoted the repulsion of the VL-loops of the PH domain away from the substrate-docking site. Similarly, the incorporation of negative charges via the phosphorylation of the Thr at position 513 has been shown to be a driving force in

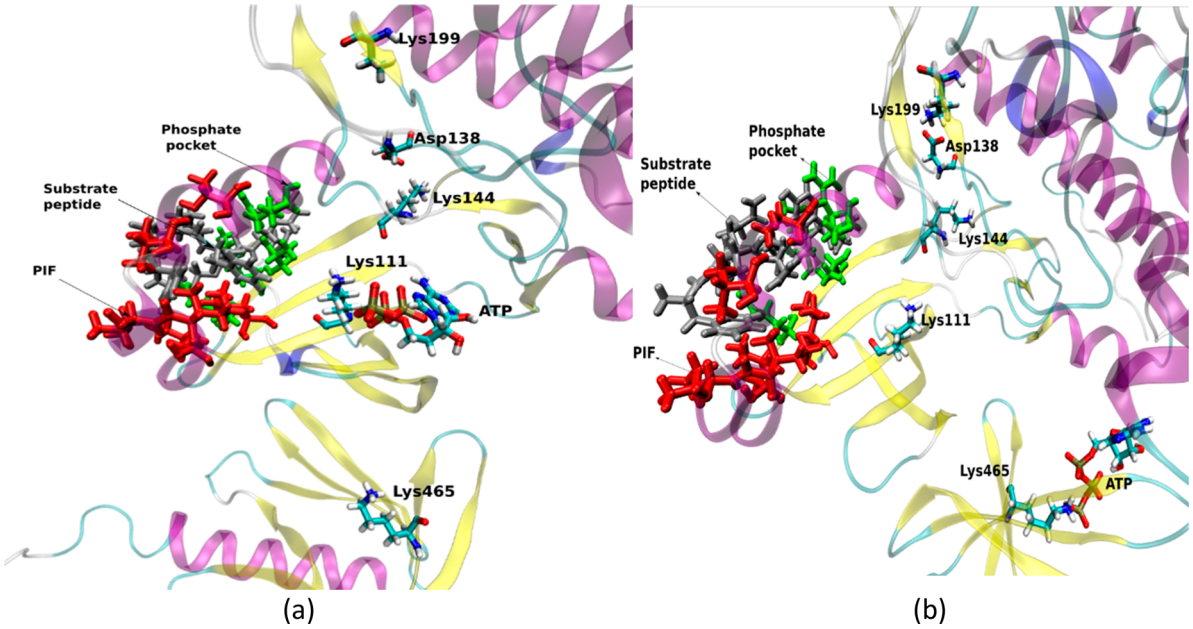

Figure 8. (a) Initial structure of the KD(5VLP)−PH(wild-type)-in complex from the MD simulation. See Figure 2 for the meanings of the colors used. (b) Final structure of the KD(5VLP)−PH(wild-type)-in complex from the MD simulation. See Figure 2 for the meanings of the colors used.

https://doi.org/10.1021/acsomega.2c02020
ACS Omega 2022, 7, 25186−25199

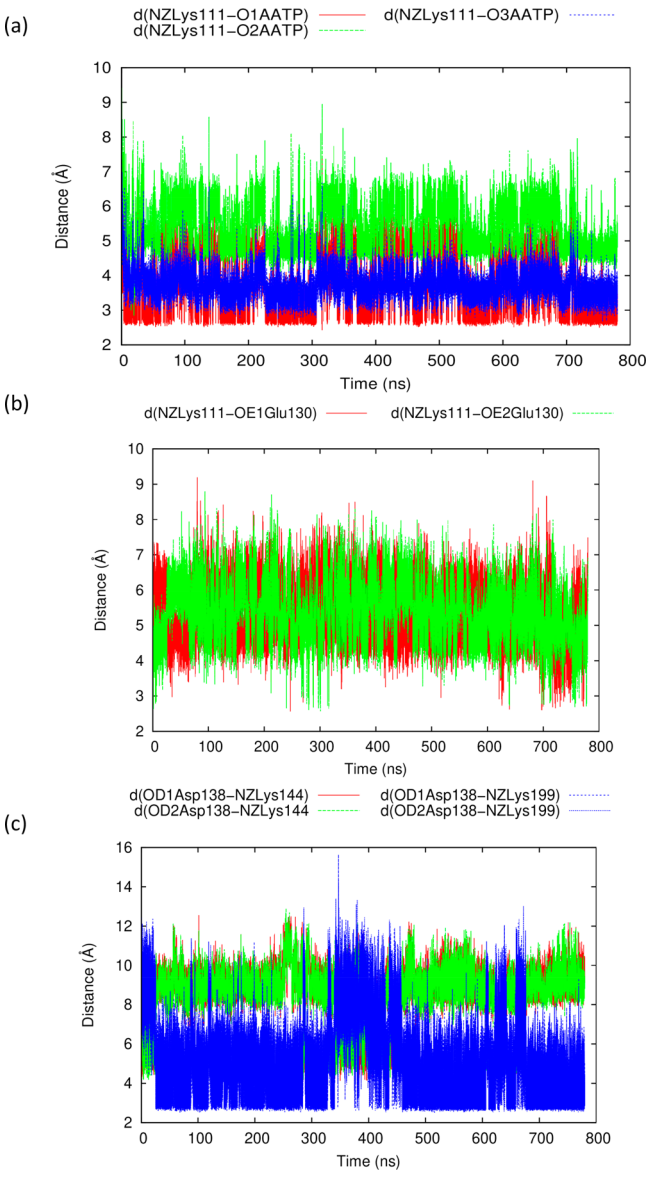

Figure 9. The KD(5LVP)−PH(K465E)-in complex. (a) Distances between Lys111 and ATP. (b) Salt bridge between Lys111 and Glu130. (c) Distances between Asp138 and Lys144 or Lys199.

PDK1 activation. As predicted by the model, this enhanced both docking site binding and catalytic activity in vivo. Thus, the theoretical results presented here for the mutant models are coherent with those obtained experimentally. In addition, our simulations shed light on phenomena that seem to characterize the active configurations (the ones represented by the PH-out wild-type and PH-in mutant models). Specifically, the more dynamical behavior of the enzyme with enhanced oscillation between the open and closed forms, which characterizes the respiration of the KD domain, as suggested by Schulze et al.,[21] and the conservation of a looser salt-bridge interaction (in comparison to the corresponding stronger interaction in the PH-in wild-type models) between Lys111 and Glu130, which is flexible enough to allow the ligand to move during catalysis.

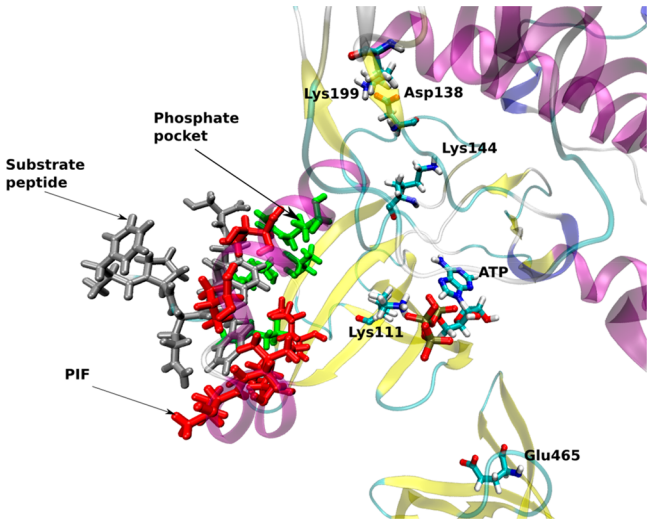

Figure 10. Final structure of the KD(5VLP)−PH(mutant K465E)-in complex from the MD simulation. See Figure 2 for the meanings of the colors used.

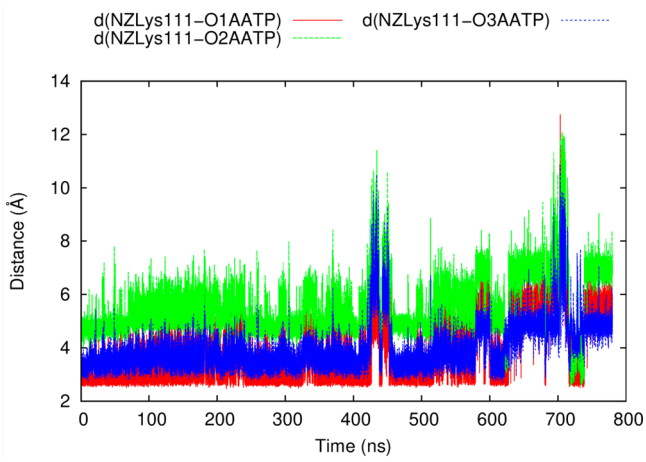

Figure 11. The KD(5VLP)−PH(wild-type)-out complex. Distances between Lys111 and ATP.

6. EXPERIMENTAL METHODS

6.1. Mice. The generation and genotyping of PDK1 K465E knock-in mice expressing the single-amino-acid substitution from Lys465 to Glu in the PDK1 PH domain were described previously.[32] Mutant mice and matched wild-type littermates were used in all the experiments. Mice were maintained on a 12 h light−dark cycle (lights on at 07:00) with ad libitum access to food and water. All animal procedures were performed in accordance with 2010/63/UE regarding the care and use of animals for experimental procedures. Protocols were approved by the Ethical Committee for Human and Animal Experimentation, Universitat Autònoma de Barcelona, and performed under a Generalitat de Catalunya Project License. The study complies with the ARRIVE guidelines developed by the NC3Rs.[59,60]

6.2. Protein Extracts. Tissues were rapidly extracted, freeze clamped in liquid nitrogen, and homogenized on ice using Kinematica Polytron (Brinkmann, CT, USA) in a 10-fold mass excess of ice-cold lysis buffer (50 mM Tris-HCl pH 7.5, 1 mM EGTA, 1% (by mass) Triton-X 100, 1 mM sodium orthovanadate, 50 mM sodium fluoride, 5 mM sodium

https://doi.org/10.1021/acsomega.2c02020
ACS Omega 2022, 7, 25186−25199

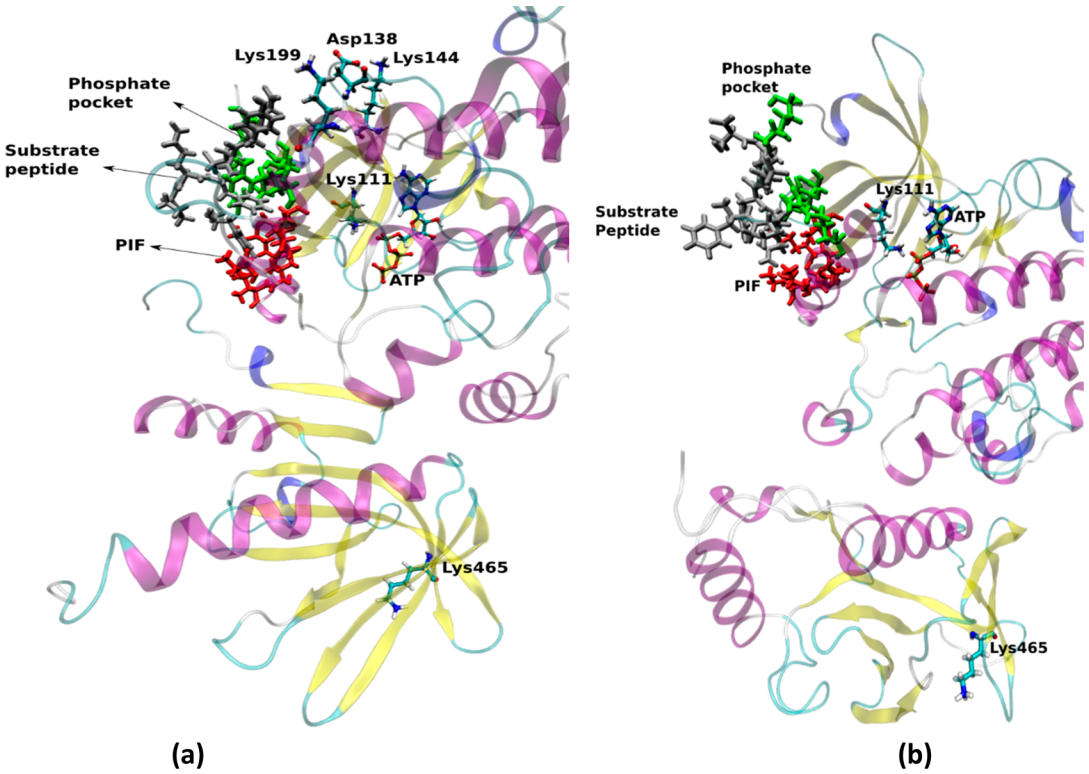

Figure 12. (a) Initial structure of the KD(5VLP)−PH(wild-type)-out complex from the MD simulation. See Figure 2 for the meanings of the colors used. (b) Final structure of the KD(5VLP)−PH(wild-type)-out complex from the MD simulation. See Figure 2 for the meanings of the colors used.

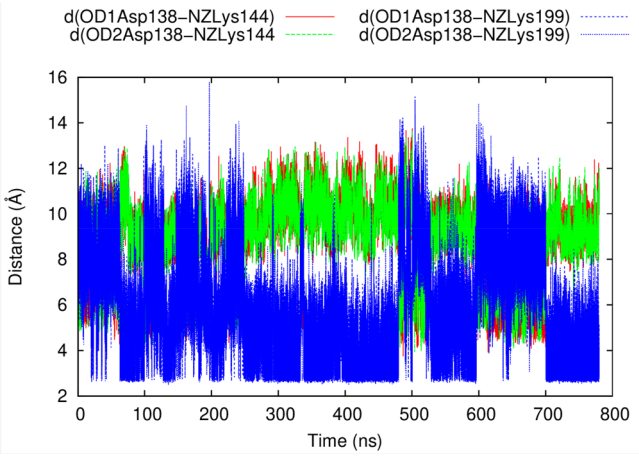

Figure 13. The KD(5LVP)−PH(wild-type)-out complex. Distances between Asp138 and Lys144 or Lys 199.

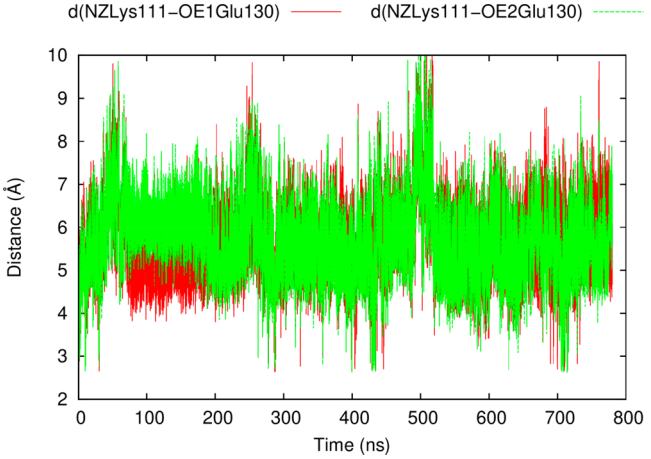

Figure 14. The KD(5LVP)−PH(wild-type)-out complex. The salt bridge between Lys111 and Glu130.

pyrophosphate, 0.27 M sucrose, 0.1% (by volume) 2-mercaptoethanol, and the complete proteinase inhibitor cocktail (one tablet per 50 mL)). Lysates were then centrifuged at 4 °C for 10 min at 13 000 × *g* to remove insoluble material. The supernatant was aliquoted, snap frozen in liquid nitrogen, and stored at − 80 °C.

6.3. Subcellular Fractionation. Tissues were rapidly extracted, freeze clamped in liquid nitrogen, and homogenized on ice using a Dounce homogenizer (50 strokes) in a 10-fold mass excess of ice-cold lysis buffer A (10 mM HEPES, 10 mM KCl, 1.5 mM MgCl2, and the complete protease inhibitor cocktail). The homogenates were centrifuged twice at 3000 × *g* for 10 min at 4 °C to remove unbroken cells and nuclei. The resulting supernatant was centrifuged at 200 000 × *g* for 60 min at 4 °C to obtain the cytosolic fraction (supernatant) and the membrane fraction (pellet), which was homogenized in buffer A containing 1% (w/v) Triton X-100.

6.4. Affinity Purification of PDK1. PDK1 was affinity purified on PIF-Sepharose from tissue lysates as described previously.[23] Briefly, 10 μL of streptavidin-Sepharose was conjugated to 0.5 μg of biotinylated PIF peptide (Biotin-C6 spacer-REPRILSE-EEQE-MFRD-FAYI-ADWC) and incubated with 0.5 mg of precleared tissue lysates at 4 °C for 1 h on a shaking platform. The pull-downs were washed twice with 1 mL of lysis buffer, resuspended in SDS sample buffer, electrophoresed and immunoblotted for PDK1.

https://doi.org/10.1021/acsomega.2c02020
ACS Omega 2022, 7, 25186−25199

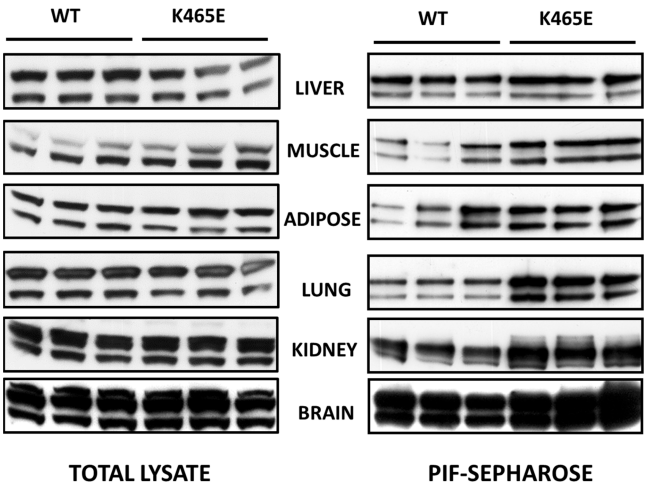

Figure 15. Protein extracts derived from the indicated tissues were obtained from PDK1 knock-in (K465E) and control wild-type (wild-type) mice. PDK1 was purified by affinity on PIF-Sepharose (right panel); as controls, PDK1 protein expression levels were measured on total tissue extracts (left panels). Representative Western blots are shown, where each lane corresponds to a sample derived from a different mouse.

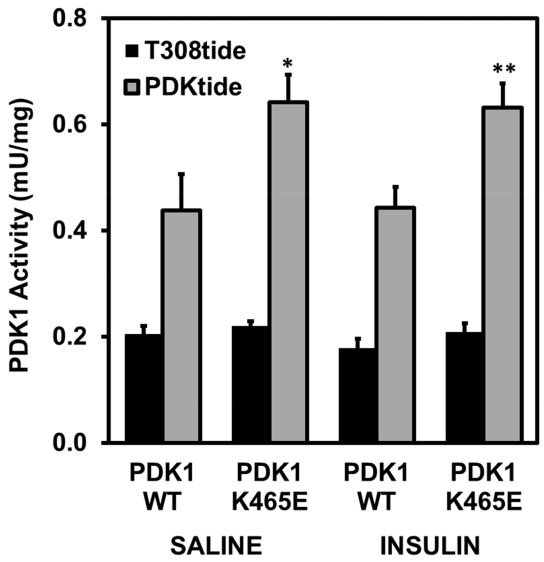

Figure 16. PDK1 was immunoprecipitated from muscle extracts of the indicated genotypes and its activity was assayed using either the T308tide or PDKtide peptides as the substrates. Each point represents the mean activity ± the standard error of the mean for three different samples, each of which was assayed in triplicate. $^{**}P < 0.005$ and $^{*}P < 0.05$ compared to controls.

6.5. Western Blot. The protein concentration was determined by the Bradford method using bovine serum albumin as the standard. Samples were electrophoresed, transferred onto nitrocellulose membranes on a Bio-Rad Mini-PROTEAN system, and immunoblotted with the indicated antibodies. The PDK1 antibody was raised in sheep against the sequence RKIQ-EVWR-QQYQ-SNPD-AAVQ, corresponding to residues 540−559 of mouse PDK1. The PKB total antibody was raised in sheep against the sequence RPHF-PQFS-YSAS-GTA, corresponding to residues 466−480 of rat PKBα. Anti-GAPDH and anti-Na-K ATPase monoclonal antibodies were from Abcam (catalogue nos. 9484 and ab7671, respectively), while the p44/42 MAPK ERK1/2 antibody was from Cell Signaling (catalogue no. 9102).

6.6. Protein Kinase Assay. The activation state of PDK1 was assessed following the immunoprecipitation of PDK1 from cell extracts. The activity was measured against the T308tide peptide (KTFC-GTPE-YLAP-EVRR, which corresponded to the T-loop of PKB, and the PDKtide, which consisted of the sequence of both T308tide and PIFtide (KTFC-GTPE-YLAP-EVRR-EPRI-LSEE-EQEM-FRDF-AYIA-DWC), as described previously.[61]

■ ASSOCIATED CONTENT

Supporting Information

The Supporting Information is available free of charge at https://pubs.acs.org/doi/10.1021/acsomega.2c02020.

Additional figures illustrating the evolution of RMSDs with time, some selected distances between relevant residues for the different KD−PH models, and a table with the calculated residence times for selected hydrogen-bond interactions (PDF)

■ AUTHOR INFORMATION

Corresponding Authors

Àngels González-Lafont − *Departament de Química, Universitat Autònoma de Barcelona, Bellaterra, Barcelona 08193, Spain; Institut de Biotecnologia i de Biomedicina (IBB), Universitat Autònoma de Barcelona, Bellaterra, Barcelona 08193, Spain;* orcid.org/0000-0003-0729-2483; Email: angels.gonzalez@uab.cat

Jose Ramón Bayascas − *Institut de Neurociències, Universitat Autònoma de Barcelona, Bellaterra, Barcelona 08193, Spain; Department of Biochemistry and Molecular Biology, Biochemistry Unit of the School of Medicine, Universitat Autònoma de Barcelona, Bellaterra, Barcelona 08193, Spain;* Email: JoseRamon.Bayascas@uab.cat

Authors

Mireia Garcia-Viloca − *Departament de Química, Universitat Autònoma de Barcelona, Bellaterra, Barcelona 08193, Spain*

José M. Lluch − *Departament de Química, Universitat Autònoma de Barcelona, Bellaterra, Barcelona 08193, Spain; Institut de Biotecnologia i de Biomedicina (IBB), Universitat Autònoma de Barcelona, Bellaterra, Barcelona 08193, Spain;* orcid.org/0000-0002-7536-1869

Complete contact information is available at: https://pubs.acs.org/10.1021/acsomega.2c02020

Notes

The authors declare no competing financial interest.

■ ACKNOWLEDGMENTS

The authors acknowledge the Spanish "Ministerio de Ciencia e Innovación" for Grants PID2020-113764GB-I00 and RTI2018-101249-B-I00

■ REFERENCES

(1) Mora, A.; Komander, D.; van Aalten, D. M. F.; Alessi, D. R. PDK1, the Master Regulator of AGC Kinase Signal Transduction. *Seminars in Cell and Developmental Biology* **2004**, *15* (2), 161−170.

(2) Pearce, L. R.; Komander, D.; Alessi, D. R. The Nuts and Bolts of AGC Protein Kinases. *Nature Reviews Molecular Cell Biology* **2010**, *11* (1), 9−22.

(3) Pawson, T.; Scott, J. D. Protein phosphorylation in signaling-50 years and counting. *Trends Biochem. Sci.* **2005**, *30* (6), 286−290.
(4) Bayascas, J. R. PDK1: the major transducer of PI 3-kinase actions. *Current Topics in Microbiology and Immunology*. **2010**, *346*, 9−29.
(5) Di Blasio, L.; Gagliardi, P.; Puliafito, A.; Primo, L. Serine/Threonine Kinase 3-Phosphoinositide-Dependent Protein Kinase-1 (PDK1) as a Key Regulator of Cell Migration and Cancer Dissemination. *Cancers* **2017**, *9* (3), 25.
(6) Arencibia, J. M.; Pastor-Flores, D.; Bauer, A. F.; Schulze, J. O.; Biondi, R. M. AGC Protein Kinases: From Structural Mechanism of Regulation to Allosteric Drug Development for the Treatment of Human Diseases. *Biochimica et Biophysica Acta (BBA) - Proteins and Proteomics* **2013**, *1834* (7), 1302−1321.
(7) Leroux, A. E.; Gross, L. Z. F.; Sacerdoti, M.; Biondi, R. M. Allosteric Regulation of Protein Kinases Downstream of PI3-Kinase Signalling. *In Advances in Experimental Medicine and Biology* **2019**, *1163*, 279−311.
(8) Sestito, S.; Chiarugi, S.; Margheritis, E.; Runfola, M.; Bertini, S.; Garau, G.; Rapposelli, S. Novel Dual PDK1/AurK-A Inhibitors for Cancer Therapy: Med Chem Evolution and Crystallographic Investigation. *Proceedings* **2019**, *22* (1), 45.
(9) Emmanouilidi, A.; Fyffe, C. A.; Ferro, R.; Edling, C. E.; Capone, E.; Sestito, S.; Rapposelli, S.; Lattanzio, R.; Iacobelli, S.; Sala, G.; Maffucci, T.; Falasca, M. Preclinical Validation of 3-Phosphoinositide-Dependent Protein Kinase 1 Inhibition in Pancreatic Cancer. *Journal of Experimental and Clinical Cancer Research* **2019**, *38* (1), 191.
(10) Gao, X.; Harris, T. K. Role of the PH Domain in Regulating in Vitro Autophosphorylation Events Required for Reconstitution of PDK1 Catalytic Activity. *Bioorganic Chemistry* **2006**, *34* (4), 200−223.
(11) Casamayor, A.; Morrice, N. A.; Alessi, D. R. Phosphorylation of Ser-241 is essential for the activity of 3-phosphoinositide-dependent protein kinase-1: Identification of five sites of phosphorylation in vivo. *Biochem. J.* **1999**, *342* (2), 287−292.
(12) Biondi, R. M. Phosphoinositide-Dependent Protein Kinase 1, a Sensor of Protein Conformation. *Trends Biochem. Sci.* **2004**, *29* (3), 136−142.
(13) Biondi, R. M.; Nebreda, A. R. Signalling Specificity of Ser/Thr Protein Kinases through Docking-Site-Mediated Interactions. *Biochem. J.* **2003**, *372* (1), 1−13.
(14) Calleja, V.; Laguerre, M.; de las Heras-Martinez, G.; Parker, P. J.; Requejo-Isidro, J.; Larijani, B. Acute Regulation of PDK1 by a Complex Interplay of Molecular Switches. *Biochem. Soc. Trans.* **2014**, *42* (5), 1435−1440.
(15) Alessi, D. R.; James, S. R.; Downes, C. P.; Holmes, A. B.; Gaffney, P. R. J.; Reese, C. B.; Cohen, P. Characterization of a 3-Phosphoinositide-Dependent Protein Kinase Which Phosphorylates and Activates Protein Kinase Bα. *Curr. Biol.* **1997**, *7* (4), 261−269.
(16) Lizcano, J. M.; Alessi, D. R. The insulin signalling pathway. *Curr. Biol.* **2002**, *12* (7), R236−238.
(17) Calleja, V.; Alcor, D.; Laguerre, M.; Park, J.; Vojnovic, B.; Hemmings, B. A.; Downward, J.; Parker, P. J.; Larijani, B. Intramolecular and Intermolecular Interactions of Protein Kinase B Define Its Activation in Vivo. *PLoS Biology* **2007**, *5* (4), e95.
(18) Ziemba, B. P.; Pilling, C.; Calleja, V.; Larijani, B.; Falke, J. J. The PH Domain of Phosphoinositide-Dependent Kinase-1 Exhibits a Novel, Phospho-Regulated Monomer-Dimer Equilibrium with Important Implications for Kinase Domain Activation: Single-Molecule and Ensemble Studies. *Biochemistry* **2013**, *52* (28), 4820−4829.
(19) Masters, T. A.; Calleja, V.; Armoogum, D. A.; Marsh, R. J.; Applebee, C. J.; Laguerre, M.; Bain, A. J.; Larijani, B. Regulation of 3-Phosphoinositide-Dependent Protein Kinase 1 Activity by Homodimerization in Live Cells. *Science Signaling* **2010**, *3* (145), ra78.
(20) Biondi, R. M.; Komander, D.; Thomas, C. C.; Lizcano, J. M.; Deak, M.; Alessi, D. R.; van Aalten, D. M. F. High Resolution Crystal Structure of the Human PDK1 Catalytic Domain Defines the Regulatory Phosphopeptide Docking Site. *EMBO J.* **2002**, *21* (16), 4219−4228.
(21) Schulze, J. O.; Saladino, G.; Busschots, K.; Neimanis, S.; Süß, E.; Odadzic, D.; Zeuzem, S.; Hindie, V.; Herbrand, A. K.; Lisa, M.-N.; Alzari, P. M.; Gervasio, F. L.; Biondi, R. M. Bidirectional Allosteric Communication between the ATP-Binding Site and the Regulatory PIF Pocket in PDK1 Protein Kinase. *Cell Chemical Biology* **2016**, *23* (10), 1193−1205.
(22) Komander, D.; Fairservice, A.; Deak, M.; Kular, G. S.; Prescott, A. R.; Downes, C. P.; Safrany, S. T.; Alessi, D. R.; van Aalten, D. M. F. Structural Insights into the Regulation of PDK1 by Phosphoinositides and Inositol Phosphates. *EMBO J.* **2004**, *23* (20), 3918−3928.
(23) McManus, E. J.; Collins, B. J.; Ashby, P. R.; Prescott, A. R.; Murray-Tait, V.; Armit, L. J.; Arthur, J. S. C.; Alessi, D. R. The in Vivo Role of PtdIns(3,4,5)P3 Binding to PDK1 PH Domain Defined by Knockin Mutation. *The EMBO Journal* **2004**, *23* (10), 2071−2082.
(24) Bayascas, J. R.; Wullschleger, S.; Sakamoto, K.; García-Martínez, J. M.; Clacher, C.; Komander, D.; van Aalten, D. M. F.; Boini, K. M.; Lang, F.; Lipina, C.; Logie, L.; Sutherland, C.; Chudek, J. A.; van Diepen, J. A.; Voshol, P. J.; Lucocq, J. M.; Alessi, D. R. Mutation of the PDK1 PH Domain Inhibits Protein Kinase B/Akt, Leading to Small Size and Insulin Resistance. *Mol. Cell. Biol.* **2008**, *28* (10), 3258−3272.
(25) Bayascas, J. R.; Sakamoto, K.; Armit, L.; Arthur, J. S. C.; Alessi, D. R. Evaluation of Approaches to Generation of Tissue-Specific Knock-in Mice. *J. Biol. Chem.* **2006**, *281* (39), 28772−2878.
(26) Currie, R. A.; Walker, K. S.; Gray, A.; Deak, M.; Casamayor, A.; Downes, C. P.; Cohen, P.; Alessi, D. R.; Lucocq, J. Role of Phosphatidylinositol 3,4,5-Trisphosphate in Regulating the Activity and Localization of 3-Phosphoinositide-Dependent Protein Kinase-1. *Biochem. J.* **1999**, *337* (3), 575−583.
(27) Lucas, N.; Cho, W. Phosphatidylserine Binding Is Essential for Plasma Membrane Recruitment and Signaling Function of 3-Phosphoinositide-Dependent Kinase-1. *J. Biol. Chem.* **2011**, *286* (48), 41265−41272.
(28) de las Heras-Martínez, G.; Calleja, V.; Bailly, R.; Dessolin, J.; Larijani, B.; Requejo-Isidro, J. A Complex Interplay of Anionic Phospholipid Binding Regulates 3′-Phosphoinositide-Dependent-Kinase-1 Homodimer Activation. *Scientific Reports* **2019**, *9*, 14527.
(29) Najafov, A.; Shpiro, N.; Alessi, D. R. Akt Is Efficiently Activated by PIF-Pocket- and PtdIns(3,4,5) *P* 3-Dependent Mechanisms Leading to Resistance to PDK1 Inhibitors. *Biochem. J.* **2012**, *448* (2), 285−295.
(30) Zhou, X.; Cordon-Barris, L.; Zurashvili, T.; Bayascas, J. R. Fine-Tuning the Intensity of the PKB/Akt Signal Enables Diverse Physiological Responses. *Cell Cycle* **2014**, *13* (20), 3164−3168.
(31) Zurashvili, T.; Cordón-Barris, L.; Ruiz-Babot, G.; Zhou, X.; Lizcano, J. M.; Gómez, N.; Giménez-Llort, L.; Bayascas, J. R. Interaction of PDK1 with Phosphoinositides Is Essential for Neuronal Differentiation but Dispensable for Neuronal Survival. *Mol. Cell. Biol.* **2013**, *33* (5), 1027−1040.
(32) Yang, S.; Pascual-Guiral, S.; Ponce, R.; Giménez-Llort, L.; Baltrons, M. A.; Arancio, O.; Palacio, J. R.; Clos, V. M.; Yuste, V. J.; Bayascas, J. R. Reducing the Levels of Akt Activation by PDK1 Knock-in Mutation Protects Neuronal Cultures against Synthetic Amyloid-Beta Peptides. *Frontiers in Aging Neuroscience* **2018**, *9* (JAN), 435.
(33) Giménez-Llort, L.; Santana-Santana, M.; Bayascas, J. R. The Impact of the PI3K/Akt Signaling Pathway in Anxiety and Working Memory in Young and Middle-Aged PDK1 K465E Knock-In Mice. *Frontiers in Behavioral Neuroscience* **2020**, *14* (May), 1−11.
(34) Santana-Santana, M.; Bayascas, J. R.; Giménez-Llort, L. Fine-Tuning the Pi3k/Akt Signaling Pathway Intensity by Sex and Genotype-Load: Sex-Dependent Homozygotic Threshold for Somatic Growth but Feminization of Anxious Phenotype in Middle-Aged Pdk1 K465e Knock-in and Heterozygous Mice. *Biomedicines* **2021**, *9* (7), 747.
(35) Sali, A.; Blundell, T. L. Comparative protein modelling by satisfaction of spatial restraints. *J. Mol. Biol.* **1993**, *234* (3), 779−815.
(36) Webb, B.; Sali, A. Comparative Protein Structure Modeling Using MODELLER. *Curr. Protoc. Bioinform.* **2016**, *54*, 5.6.1−5.6.37.

https://doi.org/10.1021/acsomega.2c02020
ACS Omega 2022, 7, 25186−25199

(37) Hindie, V.; Stroba, A.; Zhang, H.; Lopez-Garcia, L. A.; Idrissova, L.; Zeuzem, S.; Hirschberg, D.; Schaeffer, F.; Jørgensen, T. J. D.; Engel, M.; Alzari, P. M.; Biondi, R. M. Structure and Allosteric Effects of Low-Molecular-Weight Activators on the Protein Kinase PDK1. *Nature Chemical Biology* **2009**, *5* (10), 758−764.
(38) Brooks, B. R.; Brooks, C. L.; Mackerell, A. D.; Nilsson, L.; Petrella, R. J.; Roux, B.; Won, Y.; Archontis, G.; Bartels, C.; Boresch, S.; Caflisch, A.; Caves, L.; Cui, Q.; Dinner, A. R.; Feig, M.; Fischer, S.; Gao, J.; Hodoscek, M.; Im, W.; Kuczera, K.; Lazaridis, T.; Ma, J.; Ovchinnikov, V.; Paci, E.; Pastor, R. W.; Post, C. B.; Pu, J. Z.; Schaefer, M.; Tidor, B.; Venable, R. M.; Woodcock, H. L.; Wu, X.; Yang, W.; York, D. M.; Karplus, M. CHARMM: The Biomolecular Simulation Program. *J. Comput. Chem.* **2009**, *30* (10), 1545−1614.
(39) Hynninen, A.; Crowley, M. F. New Faster CHARMM Molecular Dynamics Engine. *J. Comput. Chem.* **2014**, *35* (5), 406−413.
(40) Olsson, M. H. M.; SØndergaard, C. R.; Rostkowski, M.; Jensen, J. H. PROPKA3: Consistent Treatment of Internal and Surface Residues in Empirical pKa Predictions. *Journal of Chemical Theory and Computation* **2011**, *7* (2), 525−537.
(41) Pierce, B. G.; Wiehe, K.; Hwang, H.; Kim, B. H.; Vreven, T.; Weng, Z. ZDOCK Server: Interactive Docking Prediction of Protein-Protein Complexes and Symmetric Multimers. *Bioinformatics* **2014**, *30* (12), 1771−1773.
(42) Pierce, B.; Weng, Z. ZRANK: Reranking Protein Docking Predictions with an Optimized Energy Function. *Proteins: Structure, Function and Genetics* **2007**, *67* (4), 1078−1086.
(43) Moretti, R.; Lyskov, S.; Das, R.; Meiler, J.; Gray, J. J. Web-Accessible Molecular Modeling with Rosetta: The Rosetta Online Server That Includes Everyone (ROSIE). *Protein Sci.* **2018**, *27* (1), 259−268.
(44) Case, D. A.; Babin, V.; Berryman, J. T.; Betz, R. M.; Cai, Q.; Cerutti, D. S.; Cheatham, T. E., III; Darden, T. A.; Duke, R. E.; Gohlke, H.; Goetz, A. W.; Gusarov, S.; Homeyer, N.; Janowski, P.; Kaus, J.; Kolossváry, I.; Kovalenko, A.; Lee, T. S.; LeGrand, S.; Luchko, T.; Luo, R.; Madej, B.; Merz, K. M.; Paesani, F.; Roe, D. R.; Roitberg, A.; Sagui, C.; Salomen-Ferrer, R.; Seabra, G.; Simmerling, G. L.; Smith, W.; Swails, J.; Walker, R. C.; Wang, J.; Wolf, R. M.; Wu, X.; Kollman, P. A. *AMBER 2014*; University of California: San Francisco, CA, 2014.
(45) Case, D. A.; Betz, R. M.; Cerutti, D. S.; Cheatham, T. E., III; Darden, T. A.; Duke, R. E.; Giese, T. J.; Gohlke, H.; Goetz, A. W.; Homeyer, N.; Izadi, S.; Janowski, P.; Kaus, J.; Kovalenko, A.; Lee, T. S.; LeGrand, S.; Li, P. C. Lin; Luchko, T.; Luo, R.; Madej, B.; Mermelstein, D.; Merz, K. M.; Monard, G.; Nguyen, H.; Nguyen, H. T.; Omelyan, I.; Onufriev, A.; Roe, D. R.; Roitberg, A.; Sagui, C.; Simmerling, C. L.; Botello-Smith, W. M.; Swails, J.; Walker, R. C.; Wang, J.; Wolf, R. M.; Wu, X.; Xiao, L.; Kollman, P. A. *AMBER 2016*; University of California: San Francisco, CA, 2016.
(46) Humphrey, W.; Dalke, A.; Schulten, K. VMD: Visual Molecular Dynamics. *Journal of Molecular Graphics* **1996**, *14* (1), 33−38.
(47) Jorgensen, W. L.; Chandrasekhar, J.; Madura, J. D.; Impey, R. W.; Klein, M. L. Comparison of Simple Potential Functions for Simulating Liquid Water. *The Journal of Chemical Physics* **1983**, *79* (2), 926−935.
(48) Maier, J. A.; Martinez, C.; Kasavajhala, K.; Wickstrom, L.; Hauser, K. E.; Simmerling, C. Ff14SB: Improving the Accuracy of Protein Side Chain and Backbone Parameters from Ff99SB. *Journal of Chemical Theory and Computation* **2015**, *11* (8), 3696−3713.
(49) Steinbrecher, T.; Latzer, J.; Case, D. A. Revised AMBER Parameters for Bioorganic Phosphates. *Journal of Chemical Theory and Computation* **2012**, *8* (11), 4405−4412.
(50) Berendsen, H. J. C.; Postma, J. P. M.; van Gunsteren, W. F.; Dinola, A.; Haak, J. R. Molecular Dynamics with Coupling to an External Bath. *The Journal of Chemical Physics* **1984**, *81* (8), 3684−3690.
(51) Ryckaert, J. P.; Ciccotti, G.; Berendsen, H. J. C. Numerical Integration of the Cartesian Equations of Motion of a System with Constraints: Molecular Dynamics of n-Alkanes. *Journal of Computational Physics* **1977**, *23* (3), 327−341.
(52) Darden, T.; York, D.; Pedersen, L. Particle Mesh Ewald: An N·log(N) Method for Ewald Sums in Large Systems. *The Journal of Chemical Physics* **1993**, *98* (12), 10089−10092.
(53) Deserno, M.; Holm, C. How to Mesh up Ewald Sums. I. a Theoretical and Numerical Comparison of Various Particle Mesh Routines. *J. Chem. Phys.* **1998**, *109* (18), 7678−7693.
(54) Lei, H.; Baker, N. A.; Li, X. Data-Driven Parameterization of the Generalized Langevin Equation. *Proceedings of the National Academy of Sciences of the United States of America* **2016**, *113* (50), 14183−14188.
(55) Salomon-Ferrer, R.; Götz, A. W.; Poole, D.; le Grand, S.; Walker, R. C. Routine Microsecond Molecular Dynamics Simulations with AMBER on GPUs. 2. Explicit Solvent Particle Mesh Ewald. *Journal of Chemical Theory and Computation* **2013**, *9* (9), 3878−3888.
(56) le Grand, S.; Götz, A. W.; Walker, R. C. SPFP: Speed without Compromise - A Mixed Precision Model for GPU Accelerated Molecular Dynamics Simulations. *Comput. Phys. Commun.* **2013**, *184* (2), 374−380.
(57) Johnson, D. A.; Akamine, P.; Radzio-Andzelm, E.; Madhusudan; Taylor, S. S. Dynamics of CAMP-Dependent Protein Kinase. *Chemical Reviews* **2001**, *101* (8), 2243−2270.
(58) Zhou, X.; Cordon-Barris, L.; Zurashvili, T.; Bayascas, J. R. Fine-tuning the intensity of the PKB/Akt signal enables diverse physiological responses. *Cell Cycle* **2014**, *13* (20), 3164−3168.
(59) Kilkenny, C.; Browne, W.; Cuthill, I. C.; Emerson, M.; Altman, D. G. Animal Research: Reporting in Vivo Experiments: The ARRIVE Guidelines. *Br. J. Pharmacol.* **2010**, *160*, 1577−1579.
(60) Kilkenny, C.; Browne, W. J.; Cuthill, I. C.; Emerson, M.; Altman, D. G. Improving Bioscience Research Reporting: The Arrive Guidelines for Reporting Animal Research. *PLoS Biology* **2010**, *8* (6), No. e1000412.
(61) Williams, M. R.; Arthur, J. S. C.; Balendran, A.; van der Kaay, J.; Poli, V.; Cohen, P.; Alessi, D. R. The Role of 3-Phosphoinositide-Dependent Protein Kinase 1 in Activating AGC Kinases Defined in Embryonic Stem Cells. *Curr. Biol.* **2000**, *10* (8), 439−448.

https://doi.org/10.1021/acsomega.2c02020
ACS Omega 2022, 7, 25186−25199